Computer Assisted Methods in Engineering and Science, **22**: 153–176, 2015.


# Errors of stress numerical integration for cross-sections with straight and curved boundaries

Aleksander Matuszak
*Cracow University of Technology*
*Institute for Computational Civil Engineering*
*Warszawska 24, 31-155 Cracow, Poland*
*e-mail: a.matuszak@L5.pk.edu.pl*

Internal forces are integrals of stress in a section area. Integrating the stress for an arbitrary cross-section shape and for the nonlinear stress-strain law $\sigma(\varepsilon)$ is tedious and the use of the boundary integral approach can simplify computations. Numerical integration when applied to the computations of such integrals introduces errors in many cases.

Errors of numerical integration depend on the adopted integration scheme, the type of $\sigma(\varepsilon)$ and the shape of the cross-section boundary. In the case of adaptive numerical integration what is very important are the properties of the sequence of errors produced by a given integration scheme in the increasing order of the numerical quadrature or the increasing number of subdivisions.

This paper analyses errors caused by different integration schemes for the typical $\sigma(\varepsilon)$ either for a straight or curved boundary. Special attention is paid to the properties of the error sequence in each case. The outcome of this paper is important from the viewpoint of the reliability and robustness of the software developed for nonlinear simulations of bar structures.

**Keywords:** computational mechanics, section forces, stress integration, biaxial bending, numerical integration, frame structures, nonlinear material, reinforced concrete.

## 1. Introduction

The internal forces of a bar cross-section, the normal force and bending moments in particular, are a result of the integration of the stress field over the section area. Stress distribution depends on beam deformation – elongation and curvatures, so the internal forces depend on deformation as well.

The subroutine for stress integration for a given state of deformation is one of the most fundamental subroutines in computing bar structures, i.e., beams and frames, for nonlinear materials, especially reinforced concrete.

The problems related to the integration of section internal forces are not specific to concrete, but a typical concrete constitutive model with no tension range leads to all sorts of difficulties.

The stress integration subroutine makes it possible to solve iteratively the reverse, nonlinear problem, i.e., to find the deformation that satisfies the equilibrium for given external forces, (cf. [11, 14]). Such a subroutine is also necessary for other purposes, such as a reinforced section design [14], or envelope determination (capacity contour) [1, 6, 8, 9, 16].

The subroutine for internal forces is not an independent task and it is a necessary stage in solving other problems. Moreover, internal force computations are located in the innermost loop of any nonlinear problem algorithm. Therefore, its efficiency highly influences the overall efficiency. Numerical integration can be made arbitrarily accurate but at the price of computing efficiency. What is sought then is a method that would be the most effective and sufficiently accurate at the same time. This is why so much attention is paid to this relatively simple problem. For dif-

ferent application areas, the efficiency of internal force integration affects the overall robustness differently. This influence is less strong in the case of design than in the case of optimisation or envelope. The paper provides a partial summary of the current state of the art in numerical integration.

Analytical formulae for section forces can be used for simple section shapes such as rectangular, T-shape or similar (e.g., [4, 7, 11]). In the case of complex section geometries the section may contain holes or consist of separate parts, so the methods used for numerical 2D integration (or similar [17]) are not efficient enough and the boundary integral approach is necessary. Three methods are available for expressing the area integral by the boundary integral: a) Green's theorem in global coordinates (e.g., [18]); b) Green's theorem in a rotated coordinate system (e.g., [10]); and c) the iterated integral or thin layer method [3].

Green's theorem requires $C^1$ class continuity of integrated functions. This is usually not satisfied by the stress-strain functions $\sigma(\epsilon)$ used for concrete. Therefore, the first method requires splitting the area of the section into subareas where separate branches of the stress-strain function are applied. It is a trivial task in the case of a simple section shape, e.g., a quadrilateral. However, it is much more difficult to split a geometrically complex cross-section into appropriate subareas. It requires a geometrical algorithm such as the one mentioned either by [18] or [5]. For an arbitrary section geometry, e.g., multiple connected or multipart geometry, this is a non-trivial task [12].

The second and third methods are very similar. They differ only in their underlying theory and some rather subtle issues, which are discussed in Sec. 3. In practice, both these methods can be used in a uniform manner. The integration is performed over parts of the boundary.

The boundary integral approach leads to the sum of one-variable integrals. However, for such integrals it is not possible to establish a general rule for the order of numerical integration to obtain the required accuracy.

Zupan's approach [19], in the form of the analytical integration of the appropriate function of stress, is computationally efficient and gives exact results (up to rounding errors). The drawback of this approach is that for each function $\sigma(\varepsilon)$ and for all types of boundaries (e.g., straight, curved), an appropriate set of integrals has to be implemented.

An alternative approach is to use adaptive numerical integration cf. [15]. It is particularly attractive since a single numerical integration scheme can be applied for any case of the function $\sigma(\varepsilon)$ and any shape of the boundary. The sequence of approximate values obtained by the increasing order of integration or increasing number of subdivisions is computed until the required accuracy is obtained. This approach is not very efficient but its simplicity makes it very useful, particularly in the cases where efficiency is not the primary objective. The reliability of the adaptive approach depends on the regularity and rate of convergence of the approximation sequence. It also depends on the quality of the error estimator applied for the evaluation of accuracy.

This paper includes a study of the effects of some possible numerical integration schemes and an analysis of how much the adopted scheme affects the accuracy and efficiency. The regularity and rate of convergence of the approximation sequence given by each numerical integration scheme are equally important. Error measures and error estimator properties are discussed in detail. The analysis is performed on the function $\sigma(\varepsilon)$ for concrete but its generality is restricted by the following assumptions: only normal stress is considered, no strain reversal is admitted, and reinforcement is not taken into account.

This paper is partially based on [13], and has been extended to include the part related to the integration along circular arcs.

The paper is organised as follows: first the test case, i.e., the integration of a one-variable function $\sigma(\varepsilon)$ of the type used for concrete by various integration schemes is examined. Next, the conversion of the problem from an area integral to one-variable integrals is discussed. Then, some examples of polygonal sections taken from the publications on the subject are re-examined. The last section provides an analysis of the numerical integration along a circular arc.

## 2. Integration of functions used for the approximation of the concrete constitutive relationship

The properties of numerical integration of cross-section stress are quite complex. To make the problem somewhat simpler and easier to understand, a test case is studied first in which the integration is performed over 1D domain.

Let us consider integrals of three typical functions adopted for the approximation of the concrete constitutive relationship. The considered functions contain every class of functions important from the viewpoint of numerical integration, namely polynomial functions, where the argument is raised to integer power, to real power functions and to functions which are represented by an infinite Taylor series. All functions are non-smooth at the end point of the no-tension range, some of them are also non-smooth at a point inside the compressive range. It is expected that any other function composed of such parts would not exhibit new phenomena related to numerical integration. In that sense, the considered functions are representative for concrete.

A mathematical function $y(x)$ is considered, where $y$ acts as stress and $x$ acts as strain. The considered integrals are in the form:

$$I = \int_{x_0}^{x_1} y(x)\mathrm{d}x, \tag{1}$$

where $y(x)$ is one of functions shown in Fig. 1, and the integral limits refer to the strain at maximum tension in a steel rebar and the strain at maximum compression in concrete.

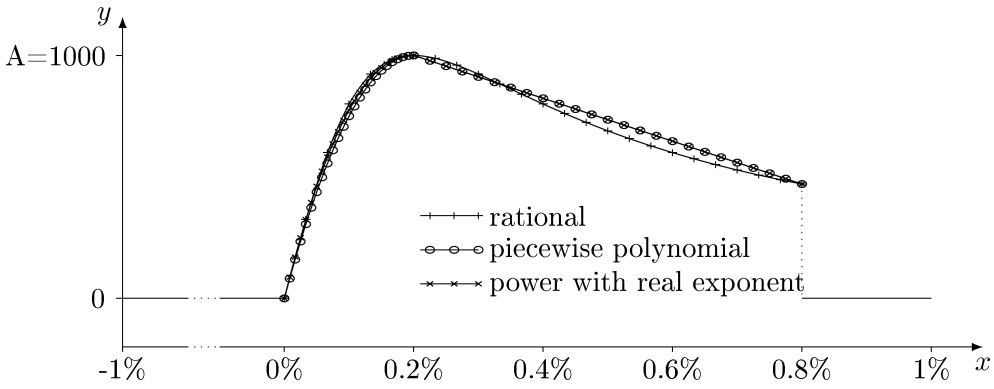


**Fig. 1.** Three functions used for approximation of concrete constitutive relationship.

The functions considered in this section are very similar (cf. Fig. 1) and are defined in the same interval, so the results of integration are similar and easy to compare. This is an important difference in comparison with the functions used in the next parts of the paper.

The first function taken into account is a rational function based on the formula of [19], with the parameters adjusted in a certain way to obtain a simpler expression.

$$y_1(x) = \begin{cases} 0 & -5a \le x < 0, \\ A\dfrac{2ax}{x^2 + a^2} & 0 \le x < 4a, \\ 0 & x \ge 4a, \end{cases} \tag{2}$$

where $a = 0.2\%$.

The second function is a piecewise polynomial:

$$y_2(x) = \begin{cases} 0 & -5a \le x < 0, \\ \dfrac{-A}{a^2}x(x-2a) & 0 \le x < a, \\ A(px+q) & a \le x < 4a, \\ 0 & x \ge 4a, \end{cases} \tag{3}$$

where $p = \dfrac{-3}{17a} \approx -88.235$ and $q = \dfrac{20}{17} \approx 1.1765$.

The last considered function is a power function with a real exponent:

$$y_3(x) = \begin{cases} 0 & -5a \le x < 0, \\ A(1-k(a-x)^{2.15}) & 0 \le x < a, \\ A(px+q) & a \le x < 4a, \\ 0 & x \ge 4a, \end{cases} \tag{4}$$

where $k = 1/a^{2.15} \approx 6.3502 \cdot 10^5$.

The exponent 2.15 is adopted here since the ascending branch of such a function fits in well between the rational and piecewise polynomial functions (see Fig. 1). Two cases of integration range are considered: the full range from $-5a$ to $4a$ and its positive part, i.e., the subrange from 0 to $4a$.

Each function given by Eqs. (2)–(4) is a piecewise-defined function, where multiple expressions define one function. Each piece of such a function is called a branch of the function to avoid confusion with another meaning of "piece" used in the text.

### 2.1. Numerical integration

For the functions specified in Eqs. (2)–(4) three possible approaches to numerical integration are compared: the first one, where the integration is over the entire domain, the second one, where the integration is over the positive subdomain, which for concrete would correspond to compressive range, and finally, the third approach is to integrate each branch of the function separately.

In each of these cases, two possible integration schemes are compared, one with an increasing number of integration points and the second one with a constant number of integration points but with a subdivision of the integration domain into equal parts.

The standard relative error, defined later (in Subsec. 3.2), is used in the comparison, and in all the figures, the scale of error is logarithmic. Attention is focused not only on errors but also on the properties of the error sequence generated by the given integration scheme.

#### *2.1.1. Increasing number of integration points*

In the first test, the integrals of these functions were calculated using Gaussian quadrature with an increasing order. The sequence of relative integration errors in both the full domain and the positive argument subrange are presented in Fig. 2.

In the case of the whole range integration (see Fig. 2a), the dependence of the integral value on the number of integration points is similar for all three functions. Figure 2a shows that the results are not very accurate.

The sequence of errors is not monotonous, it shows oscillations of decreasing amplitude, caused by derivative discontinuities. These oscillations are present up to the highest order of the quadrature.

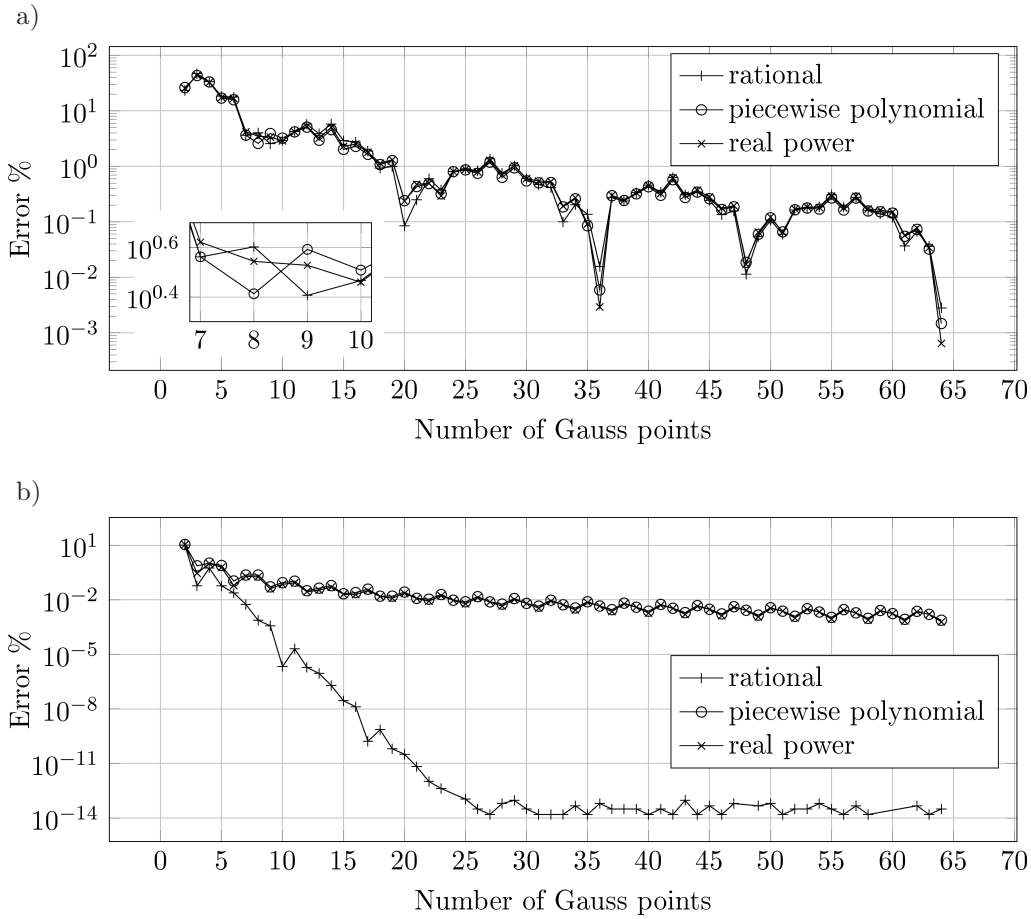


**Fig. 2.** Absolute errors of integration using Gaussian quadrature with an increasing number of Gauss points: a) full range; b) subrange for positive values.

As a result, integration with a higher number of Gauss points is not always more accurate. Therefore, the error assessment based on a comparison of either two consecutive elements of the error sequence or a doubled number of integration points is uncertain.

Integration over the full range is not used in practise. Rather, the function is integrated in the positive subrange (Fig. 2b). Consequently, the order of errors is significantly smaller, all quadratures except the two-point one give the error lower than 2%.

The properties of the numerical integration of the piecewise polynomial are different from those of polynomial, so the integral converges irregularly and despite the fact that the highest polynomial is square, even the 44-point quadrature gives the error of 0.0048%. The real power function gives almost the same error sequence as the piecewise polynomial function and it has the identical type of convergence.

For both functions the errors show small oscillations, which makes error estimation unreliable. The fact that the convergence rate is very slow is equally important. Initially, this integration scheme gives much better accuracy, but in the end the error is comparable to the error obtained for integration in the full range.

The rational function, which cannot be accurately integrated by a Gaussian quadrature, converges almost on a regular basis and the rate of convergence is high. Quadratures with more than about 26 points reach the limit of processor finite precision arithmetic, and the error oscillates around $10^{-14}$%.

This high rate of convergence makes the error estimation based on doubled number of points reliable while the estimation based on the integration with one point more is not.

These differences in type and rate of convergence are the result of differences in functions continuity. The first two functions have derivative discontinuity at $x = a$, while the third one does not have any discontinuity as it is defined by one $C^\infty$ branch.

### *2.1.2. Equal subdivision of integral range*

An alternative approach to the increase in the number of integration points is to use a constant order of integration with a subdivision of the integration interval into equal parts. This approach is very practical in programming.

In the next example, the integration range is divided into an increasing number of equal subintervals and in each subinterval, three-point Gauss integration is used. The relative errors of this integration scheme are shown in Fig. 3, both for the full range (see Fig. 3a) and the positive subrange (see Fig. 3b). In both cases, the upper integration limit is slightly shifted, which will be explained later.

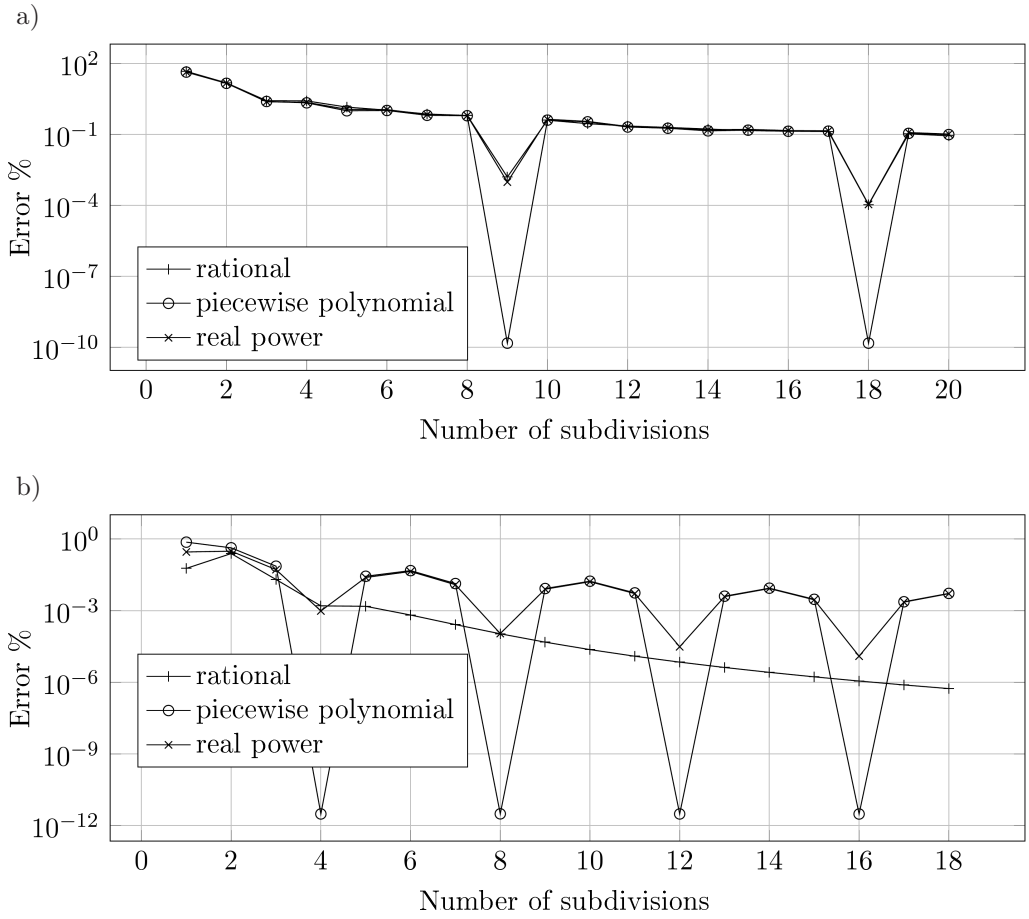


**Fig. 3.** Absolute errors of integration a using three-point Gaussian quadrature with an increasing number of subdivisions: a) full range; b) subrange for positive values.

In the case of full range integration (Fig. 3a), all three functions give almost the same sequence of errors. The sequence is quite regular, except for an essential drop for subdivisions into 9 and 18 parts. The length of the integration interval is equal to $9a$. The subdivision into a multiple of 9 equal subintervals causes the discontinuity point $x = 0$ to be located on the boundary of some subintervals. In fact, for the upper integration limit equal to $4a$ the error for the piecewise polynomial function is (numerically) zero; and this is why the upper integration limit is multiplied

by 0.999900 to make the logarithm of the error finite. This also shows that it is not necessary for point $x = a$ to be located on the boundary of the subinterval, it is enough if it is sufficiently close.

The comparison of the results for the full range and for the positive one presented in Fig. 3 shows that the order of errors is significantly smaller for the positive subrange. However, unlike the previous scheme, the integration in the full range gives a more regular sequence than in the positive range.

In this case, the length of the integration interval is equal to $4a$ and the number of subdivisions being a multiple of 4 causes the derivative discontinuity point $x = a$ for the first two functions to be located on the boundary of some subintervals.

The rational function error is not sensitive to whether the number of subintervals is a multiple of 4 and converges almost monotonically (except in the initial part). Also, the rate of convergence is high. This is the effect of the continuity of this function in the positive range.

The derivative discontinuity within the integration range may decrease the error in an unpredictable way. The chance that the error would be much lower than expected is advantageous but also makes the sequence of error irregular and any error estimation unreliable.

### *2.1.3. Integration over function branches*

The third possible approach is to integrate each branch of the function separately. In the previous example, the full range was divided into equal subdivisions, but this did not ensure that the function was smooth in these subdomains. The integral range could be divided into parts where only one branch of the function applies.

Each interval is subdivided and integrated using a three-point Gauss quadrature. Since in the rational function the positive subrange belongs to one branch, this case is therefore equivalent to the equal subdivision case (the same as in Fig. 3b). The other functions in the positive subrange have two branches and this approach is not equivalent to uniform subdivisions.

The results of this approach are shown in Fig. 4. An almost regular convergence is observed, except for the first values for the rational function, and the error is smaller than in the previous examples. It should be noted that for the piecewise polynomial function, the split of the integral domain according to function branches turns the integration of the piecewise polynomial into the integration of polynomials. For the specific function in Eq. (3), it suffices to use the two-point quadrature to obtain exact results. This is why the error for the piecewise polynomial function equals zero everywhere and therefore is not shown in Fig. 4.

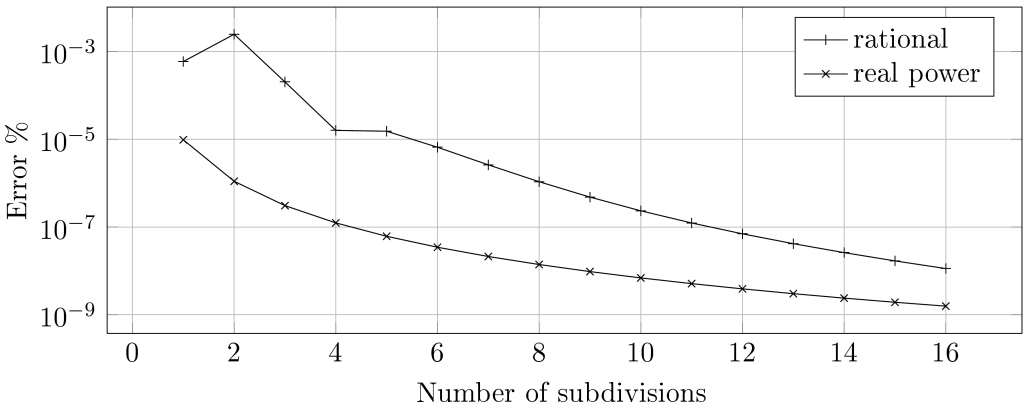


**Fig. 4.** Relative errors of an integration using a three-point Gaussian quadrature – domain split according to $\sigma(\varepsilon)$ branches and the increasing number of subdivisions for each branch.

For the real power function, the sequence of errors (Fig. 4) is monotonically decreasing and the error estimation is reliable. The rational function does not give such a regular sequence and estimating the error is not reliable.

#### *2.1.4. Function discontinuity*

The range $x \geq 4a$ is not analysed in this paper since such a state is usually not allowed in a cross-section design. Even if the range above $4a$ is not allowed for the final state, it can occur during the iterative process of equilibrium searching and the jump of the integrated function at $x = 4a$ is important for the numerical results. The function discontinuity affects the integration accuracy much more strongly than the derivative discontinuity. Consequently, the errors can be significantly greater and the sequence of errors can be more irregular.

## 3. Integration of concrete section stress

For the analysis, the Bernoulli-Euler bar is assumed. Only integration of normal stress is considered. A concrete-type material is being considered, but the problem is more general and concerns any nonlinear material. The considerations are limited to the part of internal forces resulting from the stresses in concrete. A monotonic increase of strains is assumed – a strain reversal is not admitted.

The Bernoulli-Euler assumption leads to the field of normal strains in the cross-section area:

$$\varepsilon(x,y) = \varepsilon_0 + \kappa_y x + \kappa_x y, \tag{5}$$

where the signs of the terms depend on the adopted sign convention.

The problem is to find the internal forces of the cross-section resulting from the stresses in concrete:

$$N = \int_A \sigma(x,y)\mathrm{d}A, \qquad M_x = \int_A y\sigma(x,y)\mathrm{d}A, \qquad M_y = \int_A x\sigma(x,y)\mathrm{d}A, \tag{6}$$

where $\sigma$ is an implicit function of coordinates, i.e., $\sigma = \sigma(\varepsilon(x,y))$. The positive directions of the bending moments are shown in Fig. 5, the force $F$ in the first quadrant causes positive moments. The signs of curvatures in Eq. (5) have to be consistent with the signs of moments.

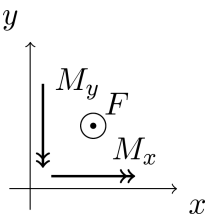


**Fig. 5.** Positive directions of bending moments, force $F$ directed upward.

### 3.1. Boundary integral

Let us consider the section in a rotated coordinate system with axes $r$, $t$ selected in such a way that $\kappa_t = 0$, then Eq. (5) becomes:

$$\varepsilon(r,t) = \varepsilon(t) = \varepsilon_0 + \kappa_r t. \tag{7}$$

In Eq. (7) the strain is dependent only on $t$ and independent of $r$; therefore, the stress becomes only one-variable function $\sigma(t)$.

Using Green's theorem, the area integral as in Eq. (6) (but now $M_r$ and $M_t$ and not $M_x$ and $M_y$) can be expressed as:

$$I = \int_A r^\alpha t^\beta \sigma(t)\mathrm{d}t\mathrm{d}r = \frac{1}{\alpha+1}\oint_\Gamma r^{\alpha+1} t^\beta \sigma\left(\varepsilon(t)\right)\mathrm{d}t. \tag{8}$$

After selecting appropriate values for $\alpha$ and $\beta$, the internal forces can be expressed as

$$N = \oint_{\Gamma} r\sigma(t)\mathrm{d}t, \qquad M_r = \oint_{\Gamma} rt\sigma(t)\mathrm{d}t, \qquad M_t = \oint_{\Gamma} \frac{1}{2}r^2\sigma(t)\mathrm{d}t, \tag{9}$$

where $r = r(t)$ is the boundary distance function, i.e., the distance from a given point of the boundary to axis $t$.

In fact, the use of Green's theorem in Eq. (8) is not admitted since this theorem requires $C^1$ continuity, and $\sigma(\varepsilon(t))$ is typically $C^0$ class at most. Equation (8) can be obtained in an alternative way without using Green's theorem [2].

Without the loss of generality, let us consider a wide strip (layer) of section area located between lines $t = t_0$ and $t = t_1$ parallel to axis $r$. The remaining bounds of the strip are provided by equations of the boundaries: right boundary $r_1(t)$, and left boundary $r_0(t)$ (cf. Fig. 6).

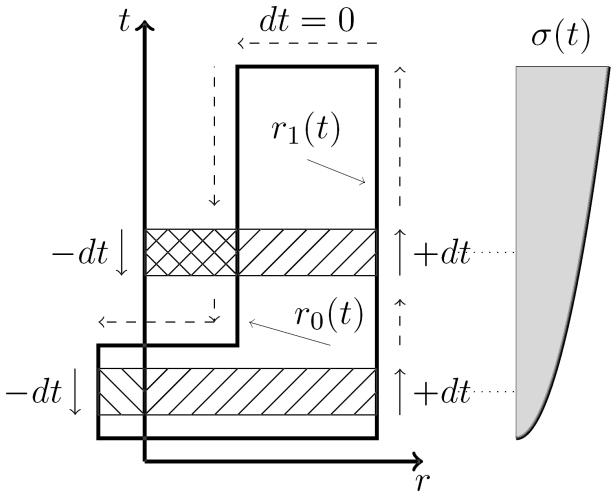


**Fig. 6.** Thin layer method and Green's theorem.

The area integral on the left-hand side (LHS) of Eq. (8) can be expressed then as an iterated integral:

$$I = \int_{t_0}^{t_1} \int_{r_0(t)}^{r_1(t)} \left(r^{\alpha} t^{\beta} \sigma(t)\right) \mathrm{d}t\mathrm{d}r. \tag{10}$$

Grouping terms independent of $r$, we obtain:

$$I = \int_{t_0}^{t_1} \left( t^{\beta}\sigma(t) \left( \int_{r_0}^{r_1} r^{\alpha}\mathrm{d}r \right) \right) \mathrm{d}t. \tag{11}$$

Dividing the inner integral into two parts leads to the interpretation of $r(t)$ as a distance to axis $t$

$$I = \int_{t_0}^{t_1} t^{\beta}\sigma(t) \left( \int_{0}^{r_1} r^{\alpha}\mathrm{d}r - \int_{0}^{r_0} r^{\alpha}\mathrm{d}r \right) \mathrm{d}t \tag{12}$$

and after integrating with respect to $r$ we obtain

$$I = \frac{1}{\alpha+1} \left[ \int_{t_0}^{t_1} r_1^{\alpha+1} t^{\beta}\sigma(t)\mathrm{d}t - \int_{t_0}^{t_1} r_0^{\alpha+1} t^{\beta}\sigma(t)\mathrm{d}t \right]. \tag{13}$$

Using the boundary orientation as in Green's theorem (cf. Fig. 6), boundary $r_1(t)$ has a positive orientation while $r_0(t)$ has a negative one. This enables us to write the integral in Eq. (13) simply as

$$I = \frac{1}{\alpha+1} \oint_{\Gamma} r^{\alpha+1} t^{\beta} \sigma(t) \mathrm{d}t. \tag{14}$$

Finally, the right-hand side (RHS) of Eq. (8) is obtained without using Green's theorem. Equation (8) derived with or without Green's theorem is identical but not equivalent. In Eq. (8), $\sigma(t)$ has to be $C^1$ continuous, while in Eq. (14) $\sigma(t)$ has to be integrable.

The use of the boundary geometry description adopted from Green's theorem greatly simplifies programming since it can handle the most complex geometries of a cross-section in a uniform way, including one consisting of separate parts as well as containing holes or composed of different material parts, such as encased steel.

The closed path integrals in Eq. (14) (as well as in Eq. (9)) lead to the sum of integrals over pieces of the boundary

$$I = \frac{1}{\alpha+1} \sum_i \int_{\Gamma_i} r^{\alpha+1} t^{\beta} \sigma(t) \mathrm{d}t. \tag{15}$$

In the most common case, where the boundary of a cross-section is composed of (or approximated by) line segments, it leads to the sum of integrals along the segments. In such a case, $r(t)$ is a linear polynomial at most.

This makes it possible to determine the appropriate order of integration for the polynomial stress-strain function. For example since the resulting polynomial for quadratic $\sigma(\varepsilon)$ in Eq. (9) is not higher than quartic, a three-point Gaussian quadrature suffices to obtain exact results.

Moreover, an alternative parametrization of the integral variable introduced by [19] can be used. As a result of Eq. (7), the relation $t(\varepsilon) = (\varepsilon - \varepsilon_0)/\kappa_r$ holds. In the case of a line segment, the dependence $r(t)$ is linear. Therefore, $r(\varepsilon)$ is also a linear function and the integral along the single edge $\Gamma_i$ to be computed in Eq. (15) can be expressed as

$$\int_{t_p}^{t_e} r^{\alpha} t^{\beta} \sigma(t) \mathrm{d}t = \sum_{\gamma=0}^{2} C_{\gamma} \int_{\varepsilon_p}^{\varepsilon_e} \varepsilon^{\gamma} \sigma(\varepsilon) \mathrm{d}\varepsilon \tag{16}$$

which makes the computation dependent only on the strain along this edge and the stress-strain function. This approach makes it possible to avoid numerical integration and to compute the exact values of corresponding integrals.

Internal forces in Eq. (9) can be considered as integrals of stress multiplied by some polynomial weighting function. The normal force is a one-variable integral of stress with a weighting function which is a linear polynomial at most, and bending moments are one-variable integrals of stress with a weighting function which is, at most, a quadratic polynomial. This makes the results of the analysis in Sec. 2 correspond (up to the scaling factor) to the normal force of the rectangular section where $r = \text{ const}$.

The analysis of the integration error for a single segment is fundamental to the analysis of the section error of internal forces. However, in the case of the sum of integrals, such an analysis is more complex than in the case of a single integral.

### 3.2. Error measure

To compare the accuracy of various integration schemes the error measure needs to be defined. At least three different measures can be used and they are not equivalent.

### 3.2.1. Local error

The most natural measure of error, and also the most common in publications on the subject, is the relative error with respect to the analytical solution:

$$\mathrm{Err}_F^i = \left| \frac{F_{\mathrm{num}}^i - F_{\mathrm{exac}}^i}{F_{\mathrm{exac}}^i} \right| \cdot 100\%, \tag{17}$$

where $F_{\mathrm{exac}}^i$ is the exact value of the integral force (axial force or bending moments) and $F_{\mathrm{num}}^i$ is its value obtained from numerical calculation. This error measure is defined for one segment and computed for each edge separately.

The error formula in Eq. (17) is a standard relative error expression. In the case of error sequence, an analysis preserving the sign of difference is useful. It provides the information on whether the approximate result is greater or less than the exact solution. For this reason, in most cases the results are presented in this paper without the absolute value in Eq. (17). However, the signed error cannot be used for a logarithmic plot.

### 3.2.2. Section error

The relative error can also be used for the total values of internal forces and defined for an entire section

$$\mathrm{Err}_F = \left| \frac{\sum F_{\mathrm{num}}^i - F_{\mathrm{exac}}}{F_{\mathrm{exac}}} \right| \cdot 100\%, \tag{18}$$

where the sum is over all segments. For the same reason as in the case of the local error, the absolute value is mostly omitted in presented examples.

### 3.2.3. Energy error

First, the global parameter is defined, which is the mechanical energy stored in the concrete part of the cross section in the form:

$$E_c = \frac{1}{2} \int_A \sigma_c \varepsilon \mathrm{d}A = \frac{1}{2}(N\varepsilon_0 + M_x\kappa_x + M_y\kappa_y). \tag{19}$$

The RHS of Eq. (19) was derived by substituting Eq. (5) into the definition of $E_c$ and using the definition of the internal forces of cross-section expressed in Eq. (6).

With this parameter, the global error can be obtained using the relative form:

$$\mathrm{Err}_E = \left| \frac{E_{\mathrm{num},c} - E_{\mathrm{exac},c}}{E_{\mathrm{exac},c}} \right| \cdot 100\%, \tag{20}$$

where $E_{\mathrm{num},c}$ and $E_{\mathrm{exac},c}$ are the values of internal energy obtained by numerical calculation and the exact value, respectively. Such a measure is nonnegative and can be 0 only when no part of the section is compressed. This simplifies detecting and handling of the error in cases when $E_c = 0$. The energy error is independent of the coordinate system.

### 3.2.4. Error estimator

The error defined by Eq. (17) or Eq. (20) requires that the exact value of the integral must be known.

Any measure of error can be converted into an error estimator by the use of a more accurate approximate value instead of the exact value, cf. [15]. Such an estimator is in fact the relative increment of two chosen elements of the approximation sequence. The choice of the element for comparison is somewhat arbitrary. The natural choice is a comparison of two consecutive elements of the sequence, but what would be the most practical is a comparison of the given element with a more distant element in the sequence, i.e., with a doubled number of integration points or doubled number of subdivisions.

The error estimator enables an automatic adaptation. Until the required relative increment is not small enough the next approximate value is computed and compared. The reliability of this approach depends on the regularity of the sequence of approximate values. A monotonically decreasing sequence ensures reliability, any irregularities may stop the adaptation before the required accuracy is obtained, e.g., two constant values in a sequence giving a relative increment equal to zero. This is why the regularity is sometimes more important than the accuracy itself.

The examples shown in Sec. 2 demonstrate that a simple integration scheme gives a very irregular sequence and the error estimation is not reliable. The more complex scheme with a split gives a monotonic sequence, except for some initial values; and after some steps it, gives reliable error estimation.

The problem of the section (global) error is more complex and will be studied in what follows.

## 4. Examples of polygonal sections

### 4.1. Rectangular cross sections

The example of numerical integration published by Fafitis [10] is referred to by many other authors and also repeated and verified by [15].

The axial force and bending moments in [10] are calculated in the coordinate system rotated about the section plastic centroid by −45°. The geometry and constitutive parabolic-rectangular relationships of the concrete are shown in Fig. 7. The integration contour is around the compressive area *b*-*a*-1-2-3-*b*.

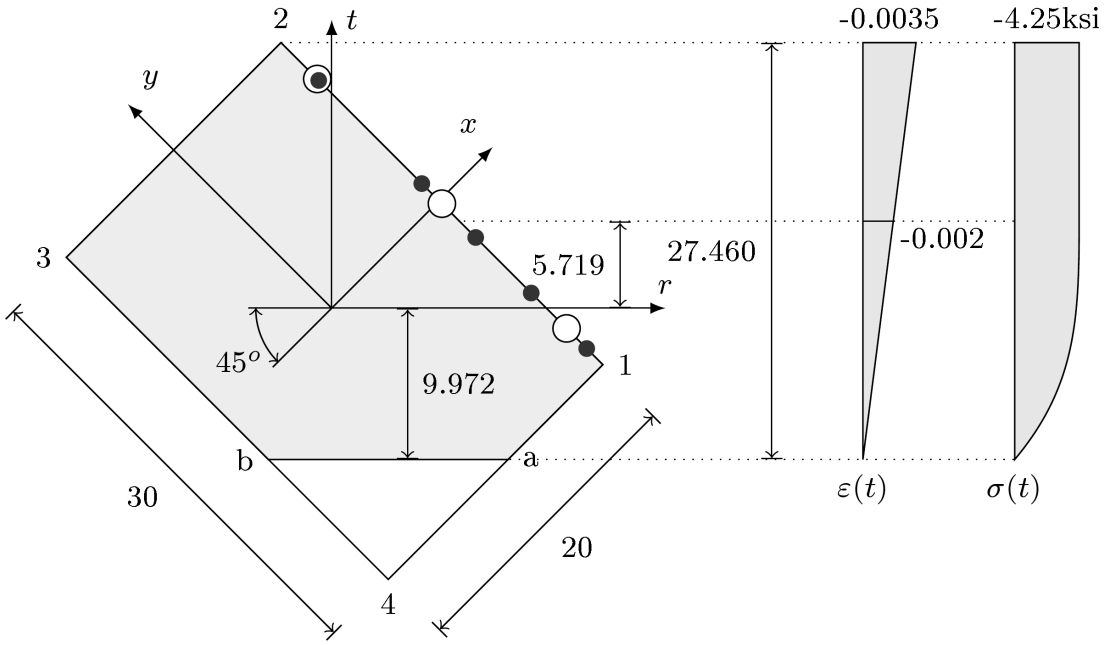


**Fig. 7.** Rectangular section analysed by Fafitis (dimensions in inches) and concrete stress-strain relationship.

Fafitis integrates stress by a three-point quadrature along each edge (e.g., big empty circles along edge 1-2). The results of these computations are not exact, since the entire compressive range is integrated by one three-point Gauss integral. However, integration in the tensile range is excluded since along edge 4-1 the integration is only over segment a-1. This corresponds to the integration scheme with no split analyzed in Subsec. 2.1.

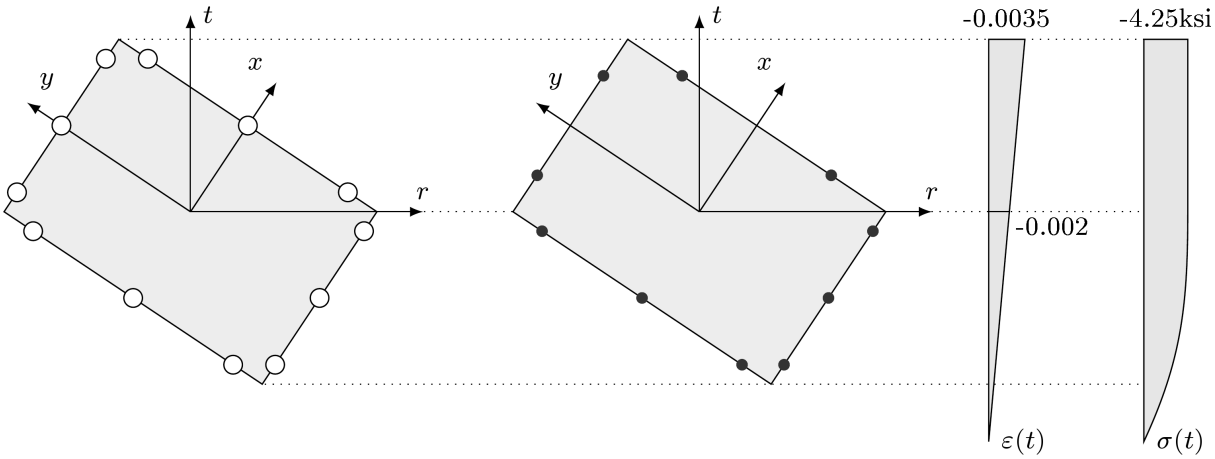


**Fig. 8.** Distribution of integration points in Fafitis approach (left) and the exact integration scheme (right) for the same section, but with a different strain distribution.

The author and co-worker [13] repeated the computations made by Fafitis because of the inconsistent rounding of values in the original paper. The results, original and repeated, are presented in Table 1 (the first two rows of each part). This is compared with the integration scheme with a split into parts where one expression for the integrand is given (filled dots along the edge 1-2). For the parabolic part of $\sigma(\varepsilon)$, a three-point quadrature was used, and for the rectangular part of $\sigma(\varepsilon)$, a two-point quadrature was used. These quadratures give exact results which could be compared with the integration scheme with a split described in Subsec. 2.1.3.

**Table 1.** Calculated internal forces resulting from concrete stress in rectangular section analysed by Fafitis.

| Edge | a-1 | 1-2 | 2-3 | 3-b | Total | Error [%] |
|---|---|---|---|---|---|---|
| axial force $N_c$ | | | | | | |
| Fafitis | −144.03 | −575.93 | −625.82 | −434.47 | −1780.25 | −0.13 |
| Author *et al.* | −143.97 | −576.26 | −625.44 | −434.43 | −1780.11 | −0.14 |
| With split | −143.97 | −452.45<br>−126.97 } − 579.42 | −461.69<br>−163.11 } − 624.80 | −434.43 | −1782.63 | 0 |
| bending moment $M_{xc}$ | | | | | | |
| Fafitis | 827.55 | −1225.89 | −5519.41 | 305.81 | −5611.94 | −0.23 |
| Author *et al.* | 827.15 | −1228.17 | −5517.13 | 305.57 | −5612.58 | −0.22 |
| With split | 827.15 | −346.42<br>−895.98 } − 1242.40 | −4779.93<br>−735.33 } − 5515.26 | 305.57 | −5624.93 | 0 |
| bending moment $M_{yc}$ | | | | | | |
| Fafitis | 1141.19 | 3460.69 | −3756.71 | −2919.30 | −2074.14 | 1.01 |
| Author *et al.* | 1140.77 | 3460.64 | −3756.69 | −2919.10 | −2074.37 | 1.03 |
| With split | 1140.77 | 3026.06<br>449.83 } 3475.89 | −2419.49<br>−1331.41 } − 3750.90 | −2919.10 | −2053.35 | 0 |

The results of computations by this method are presented in the rows labelled "with split" in Table 1. The differences are relatively small and for the engineering requirements, the results are satisfactory. It should be noted that the scheme of one quadrature over one edge leads to irregular accuracy, it is clear that one five-point integration along edge 1-2 does not have to give exact results, while the same 5 Gauss points distributed according to $\sigma(\varepsilon)$ branches gives no error at all.

Furthermore, one of the most important issues clearly shown by this example is the absence of a direct relationship between the local error and the global errors.

Let us suppose that the exact results are obtained along all edges of the section except for one edge where some error occurs. Analysing Table 1, let us investigate some possible cases. Suppose that $M_{xc}$ is computed and a 10% local error occurs along edge 2-3. This results in a global error a little below 10%. Now suppose that $M_{yc}$ is computed and a 10% local error is obtained along edge 2-3. This amplifies the global error to 18%. Finally, suppose that again $M_{xc}$ is computed but a 10% local error is obtained along edge 3-b. This results in about a 0.6% global error.

Internal forces computed by boundary integrals are the sum of terms with possibly different signs. The small relative error of each term does not guarantee that the error of their sum will be of the same order. The higher the value of the given sum component the more accurately this component should be computed. To obtain the required global level of accuracy, it is necessary to estimate each component and then determine the local error separately for each component.

In this sense, the error of numerical integration is difficult to predict and control. As long as integration is approximate, the results are susceptible to this problem.

In the case of adaptation, it leads to a very complex scheme, difficult to be programmed and containing many special cases. This is because, in general, the exact value of one of the internal forces can be zero and then a very small error along any edge results in the huge global error. Computing the relative global error with respect to total forces instead of concrete forces does not solve the problem. For example, in pure compression, the moment given by concrete is nonzero but the total moment equals zero. Furthermore, the internal forces given by reinforcement bars can be integrated exactly but those given by structural steel or FRP plates can not.

### 4.2. Error measure in different coordinate systems

The subject of the analysis is a square section $0.5 \times 0.5$ m adopted from [2] (see Fig. 9). Additionally, the following are shown in the figure: effective height $d = (a - o)(1 + \tan 15^\circ)\cos 15^\circ \approx 0.5511$ m; height of the compression zone $X = 0.2d \approx 0.1102$ m; where its projections on axes are $X_x = \dfrac{d}{\sin 15^\circ} \approx 0.4259$ m; $X_y = \dfrac{d}{\cos 15^\circ} \approx 0.1141$ m; the cover of reinforcement $o = 0.05$ m.

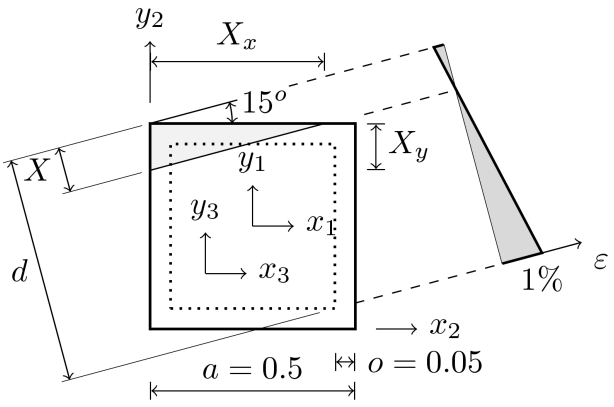


**Fig. 9.** Geometry of square section analysed by Bonet and strain distribution.

Three different coordinate systems are used, they are translated and the translation between the coordinate system $(x_1, y_1)$ and $(x_3, y_3)$ is vector $(-0.1155, -0.1155)$.

The constitutive equation is a parabola-rectangle (see Fig. 10), it can be written as follows:

$$\sigma(\varepsilon) = \begin{cases} -f_{cd}\left[1 - \left(1 - \frac{\varepsilon}{\varepsilon_{c2}}\right)^2\right] & 0 \geq \varepsilon \geq \varepsilon_{c2}, \\ -f_{cd} & \varepsilon_{c2} \geq \varepsilon \geq \varepsilon_{cu2}, \end{cases} \tag{21}$$

where the strength of concrete in compression is $f_{cd} = 25$ MPa and the characteristic strains are $\varepsilon_{c2} = -0.2\%$ and $\varepsilon_{cu2} = -0.35\%$.

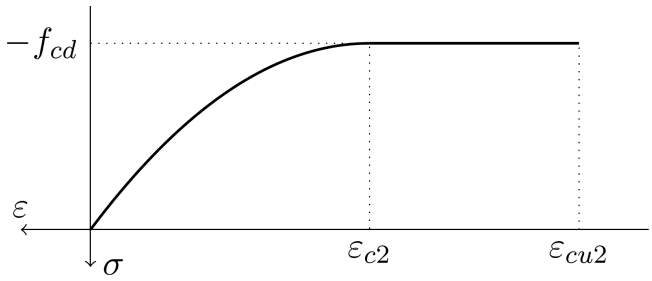


**Fig. 10.** Parabola-rectangle diagram.

For numerical integration two variants of quadrature: the two-point and three-point Gauss quadrature are used. The internal forces are computed in three different coordinate systems as shown in Fig. 9. The results are shown in Table 2.

**Table 2.** Results for the integration of the Bonet square section.

| No | Internal force/mechanical energy | Gauss quadrature | | Δ | Relative error [%] |
|---|---|---|---|---|---|
| | | 2 pt | 3 pt | | |
| coordinate system ($x_1$, $y_1$) | | | | | |
| 1 | $N$ [kN] | −348.300 | −348.300 | 0.000 | 0.000 |
| 2 | $M_x$ [kNm] | −76.045 | −76.242 | 0.197 | 0.259 |
| 3 | $M_y$ [kNm] | 45.909 | 46.645 | −0.736 | −1.578 |
| 4 | $E$ [J/m] | 193.725 | 198.045 | −4.320 | −2.181 |
| coordinate system ($x_2$, $y_2$) | | | | | |
| 5 | $N$ [kN] | −348.300 | −348.300 | 0.000 | 0.000 |
| 6 | $M_x$ [kNm] | −163.120 | −163.317 | 0.197 | 0.121 |
| 7 | $M_y$ [kNm] | −41.166 | −40.430 | −0.736 | −1.820 |
| 8 | $E$ [J/m] | 193.725 | 198.045 | −4.320 | −2.181 |
| coordinate system ($x_3$, $y_3$) | | | | | |
| 9 | $N$ [kN] | −348.300 | −348.300 | 0.000 | 0.000 |
| 10 | $M_x$ [kNm] | −123.065 | −123.262 | 0.197 | 0.150 |
| 11 | $M_y$ [kNm] | −1.111 | −0.375 | −0.736 | **−195.947** |
| 12 | $E$ [J/m] | 193.725 | 198.045 | −4.320 | −2.181 |

In this example for the integrand – a polynomial of degree four at most – a three-point quadrature gives the exact result while a two-point quadrature is sufficient for normal forces but not for bending

moments. Each three rows present values of internal forces (axial force and bending moments) as well as the absolute and relative errors for the corresponding coordinate system.

Comparing the relative errors for bending moments in the first and second systems, it is clear that the accuracy of these results is acceptable. However, the error of $M_y$ in the third system (11th row) is so huge that the results cannot be accepted.

On the other hand, when the differences of the bending moments are compared, it is noticeable that the difference for $M_x$ in each system is the same – column $\Delta$, rows: 2,6,10. The same applies to $\Delta M_y$, rows: 3,7,11.

The value of the normal force is exact and these results have a simple mechanical interpretation: the correct value of the net internal force is obtained but its location is moved to an incorrect position. This offset caused by the error is the same for each coordinate system, which means that all three of the net forces are located at the same point. Consequently, all three solutions are mechanically equivalent.

Clearly, the relative error does not reflect the mechanical properties of the solution, and the conclusions based on the relative section error can be very misleading.

The problem of the global error dependence on the coordinate system does not occur for the energy measure of the error, shown in the fourth row for each coordinate system. In all these systems, both the absolute and relative energy errors have the same value.

Unfortunately, the energy error in Eq. (20) is also the sum of the components, which is not clear from Eq. (20) itself, but the presence of the sum is the result of Eq. (15). As a consequence, some difficulties connected to global-local error relation described in Sec. 4 also apply to this error. However, the scale of the difficulties is much smaller since energy is a single quantity instead of being three components of internal forces, and the energy is always non-negative.

### 4.3. Box cross-section

In order to show the accuracy of the numerical integration of the rational stress-strain function, the rectangular cross-section with a rectangular hole considered by Zupan and Saje [19] is reanalysed. The geometry of the section is shown in Fig. 11. The strain field is given by Eq. (7) with parameters: $\varepsilon_0 = -0.001$, $\kappa_x = -0.0001$ and $\kappa_y = 0.00005$. The origin of the coordinate system is located at the bottom left-hand corner.

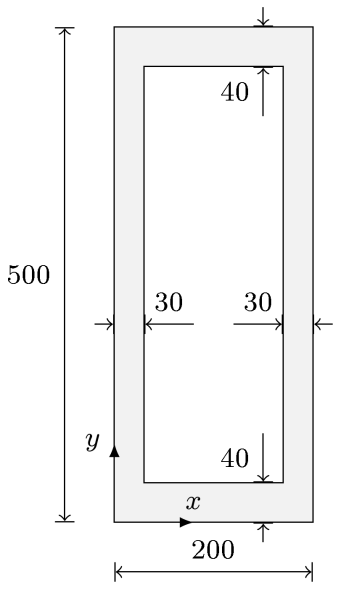


**Fig. 11.** Box cross-section analysed by Zupan and Saje.

The constitutive relationship of concrete plotted in Fig. 12 now contains a rational branch. This function can be written in the following form:

$$\sigma(\varepsilon) = \begin{cases} 0, & \varepsilon \leqslant \varepsilon_u, \\ 2f_c|\varepsilon_l|\dfrac{\varepsilon}{\varepsilon_l^2 + \varepsilon^2}, & \varepsilon_u < \varepsilon \leqslant \varepsilon_r, \\ \dfrac{\sigma_r}{\varepsilon_r - \varepsilon_m}(\varepsilon - \varepsilon_m), & \varepsilon_r < \varepsilon \leqslant \varepsilon_m, \\ 0, & \varepsilon_m < \varepsilon, \end{cases} \tag{22}$$

where $f_c = 33$ MPa is the strength of concrete in compression; $\varepsilon_l = -2.2 \cdot 10^{-3}$ is the strain obtained for $f_c$; $\varepsilon_u = -8 \cdot 10^{-3}$ is the ultimate strain in compression; $\varepsilon_r = 5.5 \cdot 10^{-5}$ is the strain obtained for the tension strength of concrete given by $\sigma_r = 2f_c|\varepsilon_l|\dfrac{\varepsilon_r}{\varepsilon_l^2 + \varepsilon_r^2}$ and $\varepsilon_m = 7 \cdot 10^{-4}$ is the ultimate strain in tension.

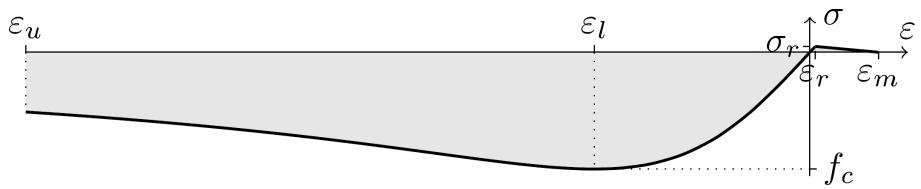


**Fig. 12.** Stress-strain relationship approximated by a rational function.

This example demonstrates the case when no exact quadrature exists for the rational function and indeed "numerical integration inherently introduces errors" [19]; therefore, the error never equals zero, which is different from the previous examples where exact values can be obtained.

The sequence of subdivisions of the integration interval has been considered and compared with the exact results obtained by the symbolic math software. The internal forces obtained by the authors for the data taken from the paper [19] differ from the ones published in that paper.

The exact value of the internal forces and relative errors can be read in Table 3. In addition, the convergence of internal forces is shown in Fig. 13.

**Table 3.** Analytical results and relative errors of the numerical integration of the section analysed by Zupan and Saje.

| Internal force/ mechanical energy | Analytical result | Relative error [%] | | | | | |
|---|---|---|---|---|---|---|---|
| | | 1 × 3 pt | 2 × 3 pt | 3 × 3 pt | 4 × 3 pt | 5 × 3 pt | 6 × 3 pt |
| $N$ [kN] | −14104.4674 | 0.308837 | 0.070491 | 0.001784 | −0.001274 | −0.000542 | −0.000186 |
| $M_x$ [kNm] | −988929.4648 | 0.552680 | 0.079102 | −0.001245 | −0.002162 | −0.000749 | −0.000236 |
| $M_y$ [kNm] | −1284356.6906 | 0.534021 | 0.151450 | 0.004087 | −0.002594 | −0.001117 | −0.000385 |
| $E$ [J/m] | 24.3885 | 0.506738 | −0.018633 | −0.007388 | −0.001335 | −0.000206 | −0.000025 |

The convergence depicted in Fig. 13 is monotonous up to four subdivisions where the error changes the sign and then the result slowly tends to the exact value below the level of practical significance. From a practical point of view, four subdivisions can be considered an accurate solution. Analytically, the error never reaches zero, but during computation on a finite precision processor this limit is reached in a finite but large number of subdivisions.

The function in Eq. (22) differs from its simplified version presented in Eq. (2) by the stress range in the tension as well as by the different location of the maximum stress for the strain value $\varepsilon_l$.

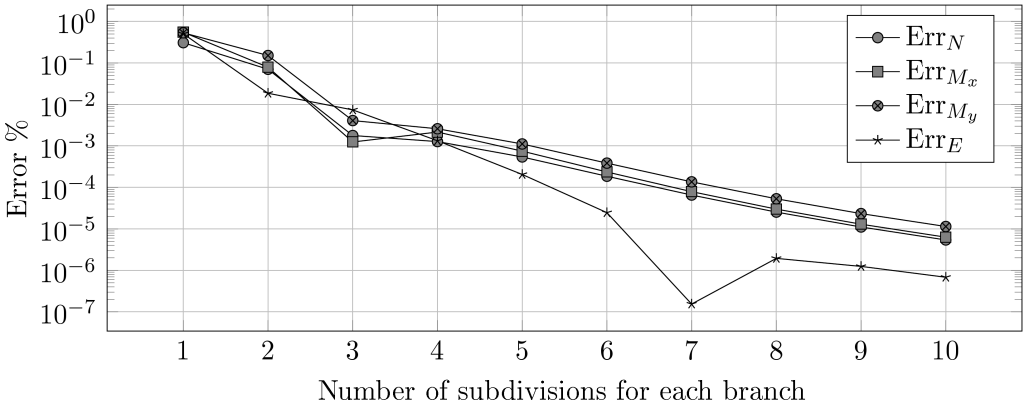


**Fig. 13.** Relative errors of the integration of the section analysed by Zupan and Saje using a three-point Gaussian quadrature in the case of a domain split according to $\sigma(\varepsilon)$ branches and an increasing number of subdivisions.

This is considered to be the reason why the type of convergence shown in Fig. 13 is qualitatively different from the type of convergence shown in Fig. 4.

Despite the high rate of convergence Fig. 4 shows that all sequences of errors display irregularities, which makes the error estimator based on a comparison of an element with the next one in a sequence unreliable.

## 5. Integration of a section with a circular boundary

The section boundary can contain parts defined by circular arcs. The ratio of the curved boundary part to the entire section boundary can change within a wide range, from a circular section, through a circular hole inside a polygonal section, to a polygon section with rounded corners. Consequently, the accuracy of the integration along a circular boundary affects the total sectional forces to a varying degree. High error along the circular boundary part could be unimportant when the circular part is a small fraction of the boundary. This is another aspect of the same effect as in global and local error relation. This implies that quite different approaches may be appropriate for sections with various ratios of the circular to polygonal boundary.

Two basic approaches can be applied: geometrical with the use of polygonal boundary approximation and analytical with the use of a curved boundary equation (see Fig. 14).

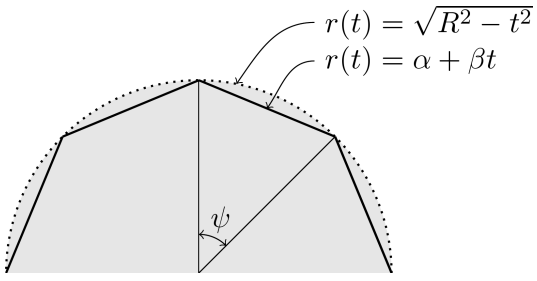


**Fig. 14.** Geometrical approximation of a section with a circular arc by a regular polygon.

To investigate properties of numerical integration along a circular arc, the extreme case of this problem, i.e., a full circle, is analysed. The full circle is divided into an increasing number of parts: equal length circular pieces of an arc. The number of parts is always selected so as to capture the four points common to the circle and the axes, so it has to be a multiple of 4. In the geometric approach, the arc is replaced by its chord (see Fig. 14). Along any part (the arc or its chord) the

numerical integration with a domain split according to $\sigma(\varepsilon)$ branches is used. With the increasing number of parts, the length of a piece of arc (or chord) decreases, the number of integration points increases and the results of the numerical integration tend to the exact value. The rate of error decreases with an increasing number of parts is investigated.

### 5.1. Geometrical approach

The geometrical approach is the simplest because the circular arc is approximated by a segment line, which leads to the use of integration methods previously described. As pointed out by [5], this approach may generate essential error. It will be shown that the nature of this error is purely geometrical.

Let us consider a circular section of radius R in uniform compression $\sigma = f_c$. The exact results are $N = \pi R^2 f_c$, $M_x = M_y = 0$ (with respect to the centre of the circle).

Figure 15 shows the relative error in normal force given by a series of circle divisions into parts, which is equivalent in this approach to circle approximation by a $4n$-side regular polygon.

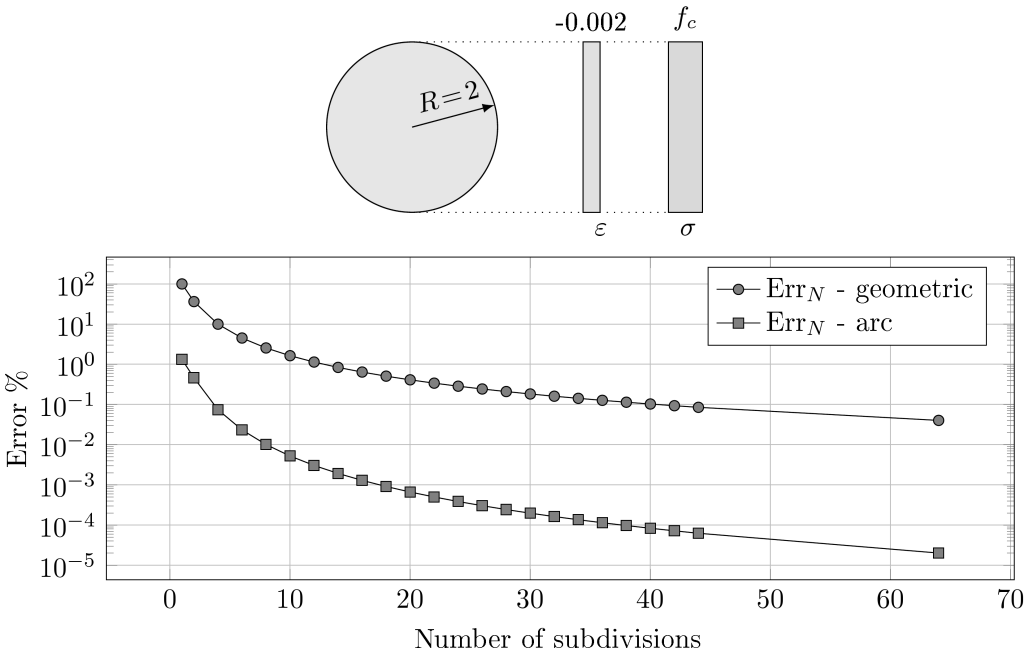


**Fig. 15.** Convergence of normal force (area of the circle) with the increasing number of parts per semicircle.

The resulting value of the normal force slowly – but very regularly – tends to the exact value. In the same way, the area of the polygon tends towards the area of the circle. It is a well-known method to compute the approximate value of $\pi$. This method is also well-known for its slow convergence.

The cases other than the uniform stress distribution can be seen as computing the "area" weighted by some functions. The weight functions in Eq. (9) are composed of a polynomial term and stress $\sigma(t)$. Weight function usually amplifies relative errors. The polynomial term is a function of distance measured from the origin and it has a large effect on the value of the integral, which primarily affects the accuracy of the calculation of the bending moments. Stress distribution can affect the result in two ways. Firstly, in the case when the most compressed section area with higher weight dominates over the lower compressed section area (see Fig. 16a). Secondly, in the case when a significant part of the section is in tension, and the weight thus equals zero (see Fig. 16b). As a result, the geometrical approximation is not sufficiently accurate (see Fig. 14) for the remaining small part of the boundary where the stress is not null.

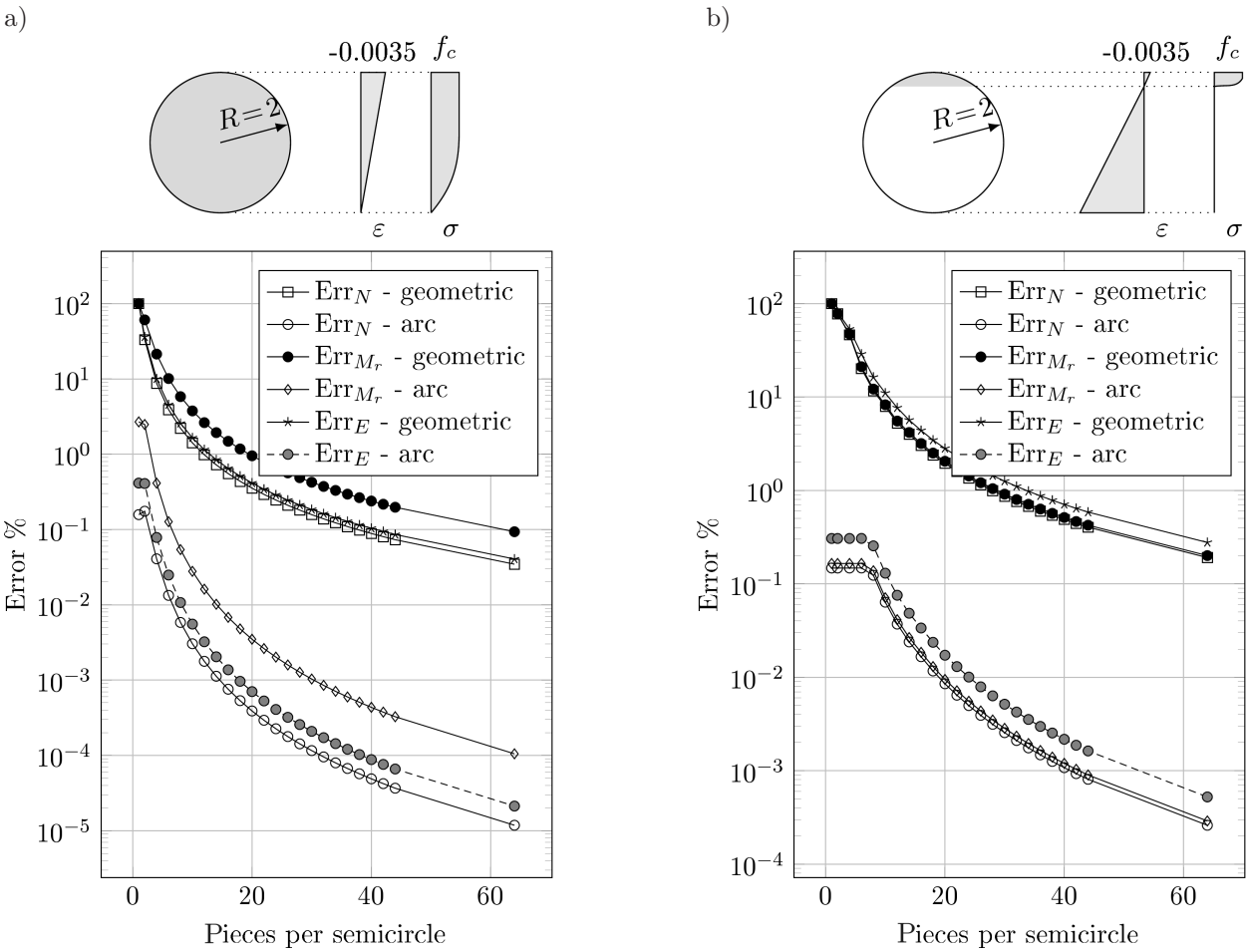


**Fig. 16.** Convergence of section forces for non-uniform strain cases with an increasing number of parts per semicircle.

The convergence of the bending moment (see Fig. 16) computed by the geometrical approach is similar to the convergence of the normal force, but the error is higher.

The geometrical approach generates either low accuracy results (for a small number of sides) or requires a long computing time.

### 5.2. Integration along a circular arc

The alternative to approximating boundary by a polygon is to use the equation of the boundary in Eq. (9). The equation of a circle boundary can be written as

$$(r - r_p)^2 + (t - t_p)^2 = R^2, \tag{23}$$

where $(r_p, t_p)$ is the centre of the circle.

For the sake of simplicity, the case of the centre of the cross section coinciding with the origin is considered, and since the section forces as in Eq. (9) are expressed as integrals with respect to $t$, the most natural way is to write the equation as $r = r(t)$

$$r(t) = \pm\sqrt{R^2 - t^2}, \tag{24}$$

where the sign depends on the side of the semicircle, whether it is located on the left or on the right side of the vertical axis. This parametrisation implies that the circular arc has to be split into

two pieces when the arc contains parts located on both sides of the vertical axis. As a consequence, parts are counted only for the semicircle.

The integrals expressing internal forces along a given circular part of the boundary have the following forms (the sign is dropped):

$$N = \int \sqrt{R^2 - t^2}\sigma(t)\mathrm{d}t, \qquad M_r = \int t\sqrt{R^2 - t^2}\sigma(t)\mathrm{d}t, \qquad M_t = \int \frac{1}{2}\left(R^2 - t^2\right)\sigma(t)\mathrm{d}t. \tag{25}$$

It should be noted that the integrand for $N$ and $M_r$ are always non-polynomial functions but the integrand for $M_t$ can be polynomial, provided that $\sigma(t)$ is polynomial.

As a consequence of this, no exact numerical quadrature for $N$ and $M_r$ exists, but for $M_t$ an exact result is obtained as long as the quadrature is exact along the line segment. It should be noted that [5] and [6] provide analytical formulae for the circular arc and parabola-rectangle $\sigma(\varepsilon)$ function.

Figure 15 also shows the comparison of the convergence ratio for the geometrical and arc approaches in the case of uniform stress distribution. The second approach is clearly superior to the first, since the two parts per semicircle arc equation approach gives about 0.5% error while the geometrical approach gives more than 35%. The arc equation approach also generates a very regular error sequence, as shown in Fig. 15.

It should also be noted that the computations with one part per semicircle are useful only for the arc equation. It corresponds to the integration along the semicircle by one quadrature, a two-point in the particular case shown in Fig. 15. The error equal to 1.3% may be acceptable in some cases. The geometrical approximation with one part leads to a trivial case: it yields a straight, vertical line and the value of the integral is equal to zero ($r(t) \equiv 0$), so the error is 100%.

Figure 16 compares the rate of convergence in both approaches in the case of non-uniform strain distributions. For the sake of simplicity, a parabola-rectangle $\sigma(\varepsilon)$ diagram according to Eq. (21) is adopted.

For cases shown in Fig. 16, instead of an analytical solution, the results refer to the result of the 256 parts per semicircle computed by the arc equation adopted as a value close enough to the exact value.

It should also be noted that each side is integrated by two-point or three-point Gauss integration and in the case of the 512 sides for a full circle, it requires the use of more than 1000 Gauss points. During the computations, a certain slow-down at the last step is noticeable.

Figure 16a shows convergence for the case of an entire section being non-uniformly compressed. The stress distribution differs essentially from the uniform one only in the lower part of the section. This non-uniform stress distribution results in $M_r$ not being equal to zero (unlike in the uniform case), and therefore, $M_r$ values clearly show integration accuracy.

In the case of the geometrical approach and division of the semicircle into two pieces, the error for $N$ is almost the same as for the uniform case (of the order 35%) but the error for $M_r$ is much higher (60%), which can be explained by the weighting term $t(r)$ in Eq. (9).

Figure 16a also shows that the convergence in all cases is similar to the one for uniform strain and stress distribution. Again the geometrical approach results in a slowly convergent series while the arc equation approach is fast convergent. All error sequences shown in Fig. 16a are very regular.

Figure 16b shows convergence for another important case when only a small part of a section is compressed, here 1/6 of the diameter. The accuracy of the geometrical approach is particularly poor, which can be explained as the effect of an inaccurate approximation of the boundary shape (see Fig. 14) in the region where the stress is not null.

An interesting effect observed in Fig. 16b should be noted: the results for a couple of initial divisions are constant. The geometrical division into equal parts is defined. The parts are next internally subdivided according to $\sigma(\epsilon)$ branches and then integrated. In this case, up to four initial divisions, and only one segment contains the entire stressed boundary and in fact the integration is performed in the same way. The fifth step divides the stressed boundary into two parts and the

results are much more accurate. The domain split according to $\sigma(\epsilon)$ branches prevents a false null result when no integration point is located in the compressed part of the boundary.

The importance of the constant value in the initial steps should be noted. This gives a relative increment equal to zero. These cases when the sequence of errors is not decreasing are the reason why, in general, the error estimator is not reliable.

Figure 16b shows that also in this case the geometrical approach gives a regular sequence of errors. The geometrical approach gives rather poor accuracy but generates a very regular sequence of errors. This makes it possible to use the geometrical approach as a reliable error estimator in cases when high accuracy is not necessary, e.g., small circular openings, small roundings of corners. In such cases, its simplicity makes it quite useful.

## 6. Conclusions

Numerical integration, in general, yields approximate results; however, particular cases when it can give exact results are computationally efficient.

The case of section force integration has problem-specific properties. Integrated functions are not $C^\infty$ continuous but the points of function or derivative discontinuity are known in advance, which is not typical in numerical integration. This makes numerical integration with no errors possible in some cases. The reasons why the numerical integration gives an approximate result could be: a) an inappropriate integration scheme, b) any branch of $\sigma(\varepsilon)$ being not a polynomial, c) a curved boundary. The function $\sigma(\varepsilon)$ and boundary shape are given; however, the integration scheme can be chosen. Integration of each branch of $\sigma(\varepsilon)$ separately requires the most complex subroutine but it leads to the best result.

Numerical integration, when not exact, involves many difficulties with accuracy assessment. The most serious difficulty is caused by the absence of a direct relationship between the local and global errors, since each section force is the sum of integrals along the segments of the boundary. These integrals can be of different signs, and a sufficiently small error of each integral (local error) does not guarantee that the error of the integrals sum (global error) will be of the same magnitude.

It was shown that the global error measure most commonly used for comparison purposes is highly dependent on the coordinate system. Therefore, without a coordinate system the value of the global error is meaningless. Also, conclusions based on global error comparison may not be true. An alternative to the global error is the energy error. This error is independent of coordinates and more suitable for accuracy assessment.

The section with parts of boundary formed by circular arcs can be integrated by conversion of the curved boundary part into piecewise line segments; but, this approach gives low accuracy results. The use of the boundary equation approach gives much more accurate results with the use of the same number of integration points.

When the numerical integration gives approximate results, it is difficult to establish *a priori* the order of numerical quadrature with acceptable accuracy, and it is necessary to investigate the sequence of errors with an increasing number of integration points or subdivisions until the stopping criterion is met. The convergence rate and regularity of such a sequence is of primary importance. The presented examples demonstrate that the increasing order of integration does not guarantee better accuracy, i.e., the error sequence is not always decreasing.

It should be stressed that an inappropriate integration scheme produces an irregular sequence of errors. Therefore it leads to the risk of stopping the adaptation with an unacceptable error.

The integration over function branches produces a much more regular error sequence but it still does not guarantee monotonically decreasing errors; therefore to be reliable, a more complex stopping criterion may be necessary. As a consequence of a high convergence rate, despite local irregularities, the sequence of relative differences of distant elements can be regular.

Unlike in the case of a fixed order of integration for a section with a curved boundary the geometrical approach gives a very regular sequence, although slowly convergent. The arc approach

gives a high rate of convergence, but regularity is not guaranteed. The slower method is more reliable than the faster one.

Due to the lack of a direct relationship between the local and global errors reaching a certain level of accuracy requires quite a complex organisation of computations, an estimation of the contribution of the given edge, to be followed by the computation of the error acceptable for the given edge, and next the adaptation of the integration to achieve this error level.

In general, the adaptive approach is not competitive with analytical integration. To be reliable, the adaptive integration requires quite a complex organization of computing, which makes this approach no longer simple. However, in particular cases one may simply extend the functionality of the existing code by a slow but reliable method.

## Acknowledgements

This scientific research has been partially financed by the project "Innovative resources and effective methods of safety improvement and durability of buildings and transport infrastructure in the sustainable development" financed by the European Union from the European Fund of Regional Development based on the Operational Program of the Innovative Economy.

The author would like to express his deep gratitude to Dr. P. Pluciński for his help. Without his support the writing of this paper would not be possible.

## References

[1] G. Alfano, F. Marmo, L. Rosati. An unconditionally convergent algorithm for the evaluation of the ultimate limit state of RC sections subject to axial force and biaxial bending. *Int. J. Numer. Meth. Eng.*, **72**(8): 924–963, 2007.

[2] J.L. Bonet, M.H.F.M. Barros, M.L. Romero. Comparative study of analytical and numerical algorithms for designing reinforced concrete sections under biaxial bending. *Comp. Struct.*, **84**(31–32): 2184–2193, 2006.

[3] J.L. Bonet, M.L. Romero, P.F. Miguel, M.A. Fernandez. A fast stress integration algorithm for reinforced concrete sections with axial loads and biaxial bending. *Comp. Struct.*, **82**(2–3): 213–225, 2004.

[4] L. Cedolin, G. Cusatis, S. Eccheli, M. Roveda. Capacity of rectangular cross sections under biaxially eccentric loads. *ACI Struct. J.*, **105**(2): 3–4, 2008.

[5] A.E. Charalampakis, V.K. Koumousis. Ultimate strength analysis of composite sections under biaxial bending and axial load. *Adv. Eng. Softw.*, **39**(11): 923–936, 2008.

[6] C.G. Chiorean. Computerised interaction diagrams and moment capacity contours for composite steel-concrete cross-sections. *Eng. Struct.*, **32**(11): 3734–3757, 2010.

[7] V. Dias da Silva, M.H.F.M. Barros, E.N.B.S. Júlio, C.C. Ferreira. Closed form ultimate strength of multi-rectangle reinforced concrete sections under axial load and biaxial bending. *Computers and Concrete*, **6**(6): 505–521, 2009.

[8] L. De Vivo, L. Rosati. Ultimate strength analysis of reinforced concrete sections subject to axial force and biaxial bending. *Comput. Method Appl. M.*, **166**(3–4): 261–287, 1998.

[9] M. Di Ludovico, G.P. Lignola, A. Prota, E. Cosenza. Nonlinear analysis of cross sections under axial load and biaxial bending. *ACI Struct. J.*, **107**(4): 390–399, July – August 2010.

[10] A. Fafitis. Interaction surfaces of reinforced-concrete sections in biaxial bending. *J. Struct. Eng. ASCE*, **127**(7): 840–846, 2001.

[11] B.A. Izzuddin, A.A.F.M. Siyam, D. Lloyd-Smith. An efficient beam-column formulation for 3D reinforced concrete frames. *Comp. Struct.*, **80**(7–8): 659–676, 2002.

[12] A. Matuszak. Algorithm for determining compressed region of cross-section and computing its moments of area. *Tech. Transact.*, **(3-B)**: 89–111, 2012.

[13] A. Matuszak, P. Pluciński. Accuracy of cross-section stress numerical integration by boundary integration formulae. In: T. Łodygowski, J. Rakowski, P. Litewka [Eds.], *Recent Advances in Computational Mechanics*, pp. 111–120. CRC Press, 2014.

[14] L. Pallarés, P.F. Miguel, M.A. Fernández-Prada. A numerical method to design reinforced concrete sections subjected to axial forces and biaxial bending based on ultimate strain limits. *Eng. Struct.*, **31**(12): 3065–3071, 2009.

[15] V.K. Papanikolaou. Analysis of arbitrary composite sections in biaxial bending and axial load. *Comp. Struct.*, **98–99**: 33–54, 2012.

[16] L. Rosati, F. Marmo, R. Serpieri. Enhanced solution strategies for the ultimate strength analysis of composite steel-concrete sections subject to axial force and biaxial bending. *Comput. Method Appl. M.*, **197**(9–12): 1033–1055, 2008.

[17] M.G. Sfakianakis. Biaxial bending with axial force of reinforced, composite and repaired concrete sections of arbitrary shape by fiber model and computer graphics. *Adv. Eng. Softw.*, **33**(4): 227–242, 2002.

[18] J.B.M. Sousa, C.F.D.G. Muniz. Analytical integration of cross-section properties for numerical analysis of reinforced concrete, steel and composite frames. *Eng. Struct.*, **29**(4): 618–625, 2007.

[19] D. Zupan, M. Saje. Analytical integration of stress field and tangent material moduli over concrete cross-sections. *Comp. Struct.*, **83**(28–30): 2368–2380, 2005.